Algebraic filters for filtered backprojection

Plantagie, L.

6

FILTERED BACKPROJECTION USING ALGEBRAIC FILTERS; APPLICATION TO BIOMEDICAL MICRO-CT DATA

Abstract – For computerized tomography (CT) imaging in (bio)-medical applications, radiation dose reduction is extremely important. This can be achieved simply by reducing the number of projection images taken. In order to obtain accurate reconstructions from few projections, however, common reconstruction techniques are not sufficient. Algebraic reconstruction methods (ARMs) are often more suited, but inflict a much higher computational burden. In this work, a recently proposed method is applied to biomedical μCT, in which the benefits of ARMs are combined with the computational efficiency of the common Filtered Backprojection (FBP) algorithm. Our experimental results demonstrate that this approach yields reconstructed images highly similar to those obtained by an ARM, while maintaining the favorable computational efficiency of FBP.

This chapter has been published with minor modification as: L. Plantagie et al. Filtered Backprojection using Algebraic Filters; Application to Biomedical Micro-CT Data. *International Symposium on Biomedical Imaging*. 2015: 1596–1599. This publication is available through http://dx.doi.org/10.1109/ISBI.2015.7164185.

6.1 INTRODUCTION

Computerized tomographic (CT) imaging has many applications in clinical settings, in (bio)medical research, and in industry. In this chapter, we focus on the biomedical imaging task. For example, in osteoporosis research, reconstructions from μCT scanners are commonly used to perform a longitudinal analysis on the bone structures of small animals subjected to some form of treatment [1]. Due to the harmful nature of X-rays, radiation dose reduction is an important research goal for the community. One common way of reducing radiation is simply to take fewer projection images. This requires reconstruction methods that can handle such datasets well.

Two main types of reconstruction methods exist in the literature. *Analytical reconstruction methods* are based on a discretization of an exact inversion formula for the reconstruction problem. Well-known methods of this type are *Filtered Backprojection (FBP)* and *Feldkamp-David-Kress (FDK)*. These methods perform a filtering step of the measured data in the Fourier space with a predefined filter. Many standard filters are known from literature, such as the Ram-Lak, Hann and Cosine filter [2]. The optimal filter depends on the characteristics of the projection data, such as the signal to noise ratio and the number of projection angles. The main advantage of analytical methods is their high computational efficiency, which is why they are offered in nearly all commercial CT-scanner packages [3]. The downside of these methods, however, is their inflexibility to special scanning geometries and its inability to deal with insufficient data (e.g. when only few projections images are available).

Algebraic reconstruction methods (ARM) are typically much more robust with respect to incomplete or noisy projection data, due to their inherent ability to model the actual projection geometry of the scanning device. ARMs, such as SIRT, ART and CGLS [4], which compute a reconstruction by applying a sequence of update iterations, generally converge to a solution that is optimally consistent with the measured data, with respect to some norm. The drawback of these methods is their heavy computational burden compared to analytical methods. Moreover, the rapid improvement in detector technology is leading to ever larger volume sizes (i.e. higher resolution reconstructions) much faster than the advances in computational hardware can keep up with. Ideally therefore, one would like to combine the computational requi-

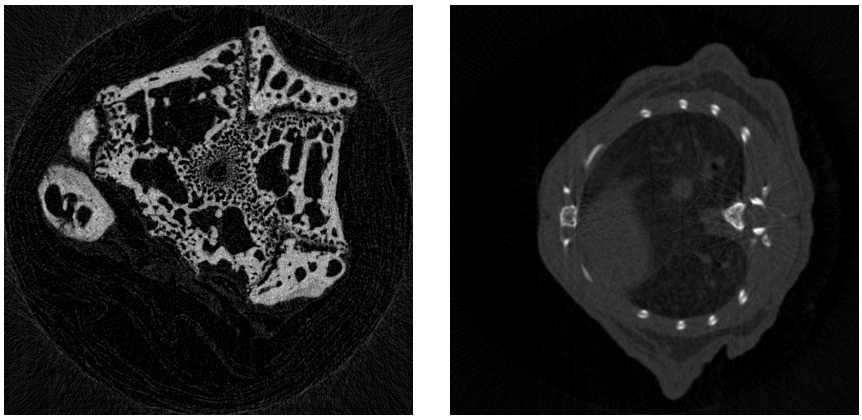

(a) Rat femur (b) Mouse thorax

Figure 6.1: FBP reconstructions of two μCT scans using (a) 360 projection angles; (b) 225 projection angles.

rements of analytical methods with the robustness of algebraic methods. In [5], a method was described for developing filters for analytical methods that are based on the convergence behavior of a linear ARM. The reconstructions of FBP with these filters approximate the reconstructions of the corresponding ARM.

Many other methods have been developed to create optimal filters for FBP. Here, we mention only some recent work in the field. In [6], Zeng derives a filter in the frequency domain based on the Landweber algorithm. Nielsen et al. derive filters specifically for a tomosynthesis geometry [7]. Pelt and Batenburg use artificial neural networks to find good filters based on prior knowledge for datasets with a small number of projection angles [8]. They also provide a method to find filters such that the projection error is minimal [9]. In [10], Kunze et al. describe a method that also approximates an ARM. Opposed to the method described in [5], Kunze et al. need objects to obtain their filters.

In this chapter, we will apply the method from [5] to two sets of biomedical μCT data, that are acquired from a rat femur and a mouse thorax respectively. We aim to show the resemblance between SIRT and FBP that is obtained by using the custom filters from [5]. Reconstructions of the scanned objects using many projection angles are shown in

Fig. 6.1, where a display range was chosen to enhance visibility. The same range is used for all reconstructions in this chapter.

This chapter is structured as follows. In Sec. (6.2), the method from [5] is briefly described. Sec. (6.3) contains information on acquiring the experimental data and the experiments that are performed. The results are shown in Sec. (6.4). We discuss our findings and conclude this chapter in Sec. (6.5).

6.2 THE AF-FBP METHOD

This section contains a brief discussion of the *Algebraic Filter - Filtered Backprojection (AF-FBP)* reconstruction method. We first consider the Filtered Backprojection method and then explain the reasoning behind creating filters based on a linear ARM. For simplicity, we consider only a 2D parallel beam setup, but the concepts can be extended to other geometries as well.

FBP is a discretization of the inverse Radon transform, where the projection data $\mathbf{p}$ is filtered by a filter g and then backprojected. The filter $g : \mathbb{R}^2 \to \mathbb{R}$ can be chosen freely, depending on the experimental setup. The reconstruction formula for FBP is given by Eq. (6.1).

$$f(x, y) = \sum_{\theta \in \Theta} \sum_{\tau \in T} p_{\theta\tau} g(\theta, \tau - x\cos\theta - y\sin\theta), \tag{6.1}$$

where $f : \mathbb{R}^2 \to \mathbb{R}$ is the unknown image, Θ denotes the set of projection angles, T denotes the set of detector bins and $\mathbf{p} \in \mathbb{R}^m$ with $m = |\Theta| \cdot |T|$.

The AF-FBP method generates angle-dependent filters g based on the convergence of a linear ARM [5]. For this chapter we use the iterative method SIRT. Since SIRT is a linear, stationary Richardson solver, there exists a reconstruction matrix $\mathbf{R} : \mathbb{R}^m \to \mathbb{R}^n$ such that, for a fixed number of K iterations, the reconstruction $\mathbf{u} \in \mathbb{R}^n$ of SIRT is given by $\mathbf{u} = \mathbf{R}\mathbf{p}$. By writing this equation element wise for a certain pixel c of $\mathbf{u}$, we obtain Eq. (6.2).

$$u_c = \sum_{\theta \in \Theta} \sum_{\tau \in T} r^{(c)}_{\theta\tau} p_{\theta\tau}, \tag{6.2}$$

where $r^{(c)}$ denotes the cth row of $\mathbf{R}$.

Let the coordinates of the center of pixel c be denoted by $(x_c, y_c) \in \mathbb{R} \times \mathbb{R}$, then $t_c^{(\theta)} = x_c \cos\theta + y_c \sin\theta$ is the projection of pixel c on the detector at angle θ. For a variable $\tau \in T - t_c^{(\theta)}$, where the minus sign denotes element wise subtraction, we define a function $h^{(c)} : \mathbb{R}^m \to \mathbb{R}$ by Eq. (6.3).

$$h^{(c)}(\theta, \tau) = r^{(c)}_{\theta(\tau + t_c^{(\theta)})}. \tag{6.3}$$

Combining Eq. (6.2) and Eq. (6.3) yields the formula in Eq. (6.4).

$$u_c = \sum_{\theta \in \Theta} \sum_{\tau \in T} p_{\theta\tau} h^{(c)}(\theta, \tau - x_c \cos\theta - y_c \sin\theta). \tag{6.4}$$

Hence for the central pixel c, the role of function $h^{(c)}$ equals that of the filter g in Eq. (6.1). It has been shown in [5] that, for pixel c being the pixel at the center of the image grid, the use of the function $h^{(c)}$ as a filter in the FBP method yields a good approximation of the linear ARM. We refer to $h^{(c)}$ as an *algebraic filter*.

Each coefficient of the algebraic filter can be obtained by applying SIRT to projection data $\mathbf{p}$ that equals a unit vector $\mathbf{e}_{\theta\tau}$, with entry one on position $\theta\tau$ and zero otherwise. The resulting image pixel u_c will then equal $r^{(c)}_{\theta\tau}$; see also Eq. (6.2). After applying this step for all unit vectors $\mathbf{e}_{\theta\tau}$ with $\theta \in \Theta$ and $\tau \in T$, the algebraic filter $h^{(c)}$ can now be deduced from $r^{(c)}$ by using Eq. (6.3).

The algebraic filter $h^{(c)}$ can be applied to projection data in the same way as standard filters that are often used for FBP.

6.3 EXPERIMENTS

In this section, we describe experiments that we performed and define the measure that we use to examine the image quality of the reconstructions.

We consider the central slices of the two datasets depicted in Fig. 6.1. As the method AF-FBP is deduced for a parallel beam scanning geometry, the central slices were rebinned to parallel beam projection data. The first dataset concerns an ex-vivo scan of a rat femur, cross-sectioned at the epiphyseal plate, an area of interest for femur research. In total, 376 projection images were taken with a resolution of 5µm in

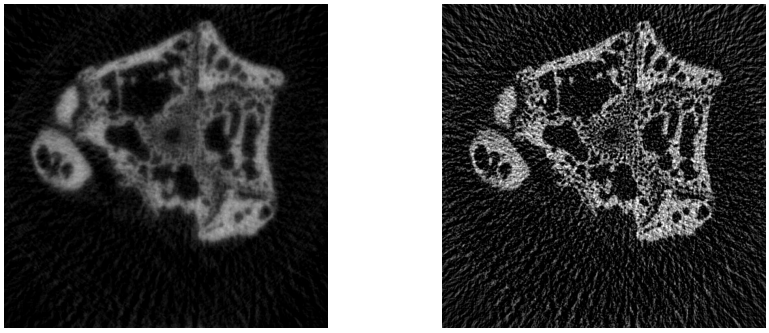

(a) SIRT (b) FBP-Hann

Figure 6.2: Reconstructions of femur projection data with 60 projection angles and SIRT with $K = 50$ iterations.

a Bruker μCT SkyScan 1172 scanner running at 40kV. The second dataset concerns an in-vivo scan of a mouse, cross-sectioned at the thorax. Its 451 projections of resolution 34μm were taken in a Bruker μCT SkyScan 1076 system running at 59kV. For both datasets, the SkyScan NRecon software was used for data preprocessing and beam hardening correction. To emulate low dose scans, we selected 45 and 60 projection angles from both scans.

In the experiments, we apply the SIRT-FBP method (FBP with an algebraic filter based on SIRT) to the above mentioned datasets. The aim of SIRT-FBP is to approximate the SIRT reconstruction. We will first consider the reconstructions of SIRT and FBP with a standard filter. They are shown for the femur dataset in Fig. 6.2, where SIRT is performed with $K = 50$ iterations and the Hann filter is chosen as the standard filter for FBP. The reconstructions of SIRT and FBP-Hann (FBP with a standard Hann filter) have characteristic imaging features. The SIRT reconstruction is a smoothed image, while the FBP-Hann reconstruction contains extensive streaking artifacts. Furthermore, the heavy computational burden of SIRT can be a reason to choose FBP, even when a researcher would favor the reconstruction quality of SIRT over FBP. In those situations, SIRT-FBP could be applied, which yields an approximation of SIRT with comparable computation time as FBP with standard filters.

In all experiments, the number of detector bins is $D = 799$. The reconstruction grid is a square, consisting of $D \times D$ pixels of unit size. The number of iterations for SIRT is $K = 50$, unless stated differently. The forward projections that are needed to execute SIRT are obtained using the Joseph kernel [11]. For the calculations in this chapter we use the ASTRA toolbox [12].

6.3.1 *Quality measure*

The quality of the reconstructions is examined by comparing the reconstructions with the SIRT reconstruction, since the aim of SIRT-FBP is to approximate SIRT. The reconstructions are compared on the reconstruction grid of $D \times D$ pixels. Denote a reconstruction by $\mathbf{u} = (u_{kl})$ with $1 \leqslant k, l \leqslant D$. Furthermore, let the algebraic reconstruction be denoted by $\mathbf{u}^{\mathrm{ARM}} = (u_{kl}^{\mathrm{ARM}})$. Then the *mean ARM reconstruction error* is defined as

$$E_r^{\mathrm{ARM}} = \frac{\sum_{k,l} |u_{kl} - u_{kl}^{\mathrm{ARM}}|}{\sum_{k,l} u_{kl}^{\mathrm{ARM}}}. \tag{6.5}$$

Hence E_r^{ARM} is an L_1-norm in the object space combined with a scaling term. We assume that the set of projection data is nonnegative and that $\mathbf{u}^{\mathrm{ARM}}$ is nonzero.

6.4 RESULTS

In this section, we show the results of the experiments described in Sec. (6.3). We emphasize that the purpose of AF-FBP is to approximate the quality of the corresponding ARM reconstructions, instead of improving the overall reconstruction quality.

In Fig. 6.3 we show the reconstructions of the femur dataset for SIRT, SIRT-FBP, FBP-RL (FBP with a standard Ram-Lak filter) and FBP-Cos (FBP with a standard Cosine filter). The number of projection angles is $d = 60$ and the number of SIRT iterations is $K = 50$. For the reconstruction of FBP-Hann (FBP with a standard Hann filter) we refer to Fig. 6.2. Notice the resemblance between the SIRT and SIRT-FBP reconstruction, and the streak artifacts for FBP-RL and FBP-Cos which are much more pronounced.

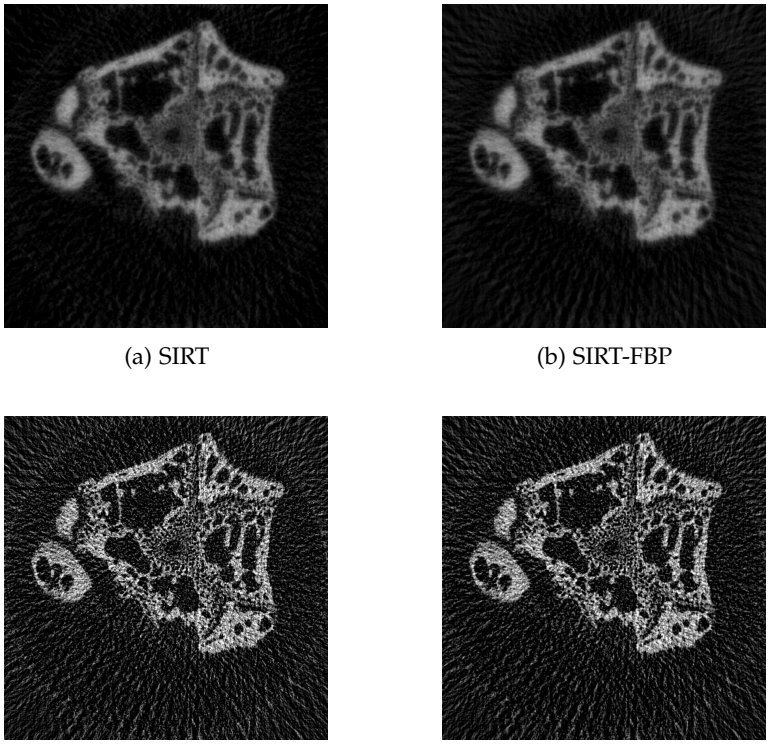

(a) SIRT (b) SIRT-FBP

(c) FBP-RL (d) FBP-Cos

Figure 6.3: Reconstructions of femur projection data with 60 projection angles and SIRT with $K = 50$ iterations.

We use the mean ARM reconstruction error (see Sect. 6.3.1) to compare the reconstructions. The results are shown in Table 6.1. The E_r^{ARM} for SIRT-FBP is significantly smaller than that of FBP with standard filters. This implies that SIRT-FBP approximates the SIRT reconstruction, while FBP reconstructions with standard filters differ substantially from SIRT reconstructions.

We obtain similar results for a different number of iterations K in the range from 10 to 1000, although the differences in E_r^{ARM} decrease for increasing K.

Class	*SIRT-FBP*	*FBP-RL*	*FBP-Hann*	*FBP-Cos*
45 projection angles				
femur	0.18	1.6	1.3	1.4
thorax	0.13	0.50	0.43	0.46
60 projection angles				
femur	0.17	1.3	1.1	1.2
thorax	0.12	0.42	0.36	0.38

Table 6.1: Mean ARM reconstruction errors E_r^{ARM} for $K = 50$.

6.5 CONCLUSIONS AND DISCUSSION

We introduced the method AF-FBP, which uses custom filters that are created based on a linear ARM. The reconstructions of AF-FBP approximate the reconstructions of the ARM that was used to create the filters. This was already shown in earlier work for simulated data [5]. In this work, we have applied this new method to experimental biomedical μCT data for the first time. Our results demonstrate that reconstructions approximating the image quality of SIRT can now be created with the computationally fast FBP method.

In this chapter we have focused on the image quality of AF-FBP compared to SIRT, because SIRT-FBP is designed to approximate SIRT. Whether it is advantageous to use SIRT (or SIRT-FBP) instead of FBP with other filters depends on the application and the features that are desirable for the particular imaging task. In future work, we will investigate how other algebraic methods – that are capable of incorporating prior knowledge or particular noise models – can be approximated following a similar approach.

BIBLIOGRAPHY

[1] E. Perilli et al. Detecting early bone changes using in vivo micro-CT in ovariectomized, zoledronic acid-treated, and sham-operated rats. *Osteoporosis International* 2010; 21(8): 1371–1382.

[2] A. C. Kak and M. Slaney. *Principles of Computerized Tomographic Imaging*. Philadelphia: SIAM, 2001.

[3] X. Pan, E. Y. Sidky, and M. Vannier. Why do commercial CT scanners still employ traditional, filtered back-projection for image reconstruction? *Inv. Problems* 2009; 25(12): 123009.

[4] J. Gregor and T. Benson. Computational analysis and improvement of SIRT. *IEEE Trans. Med. Imag.* 2008; 27(7): 918–924.

[5] K. J. Batenburg and L. Plantagie. Fast Approximation of Algebraic Reconstruction Methods for Tomography. *IEEE Trans. Image Process.* 2012; 21(8): 3648–3658.

[6] G. L. Zeng. A filtered backprojection algorithm with characteristics of the iterative Landweber algorithm. *Med. Phys.* 2012; 39(2): 603–607.

[7] T. Nielsen et al. Filter Calculation for X-Ray Tomosynthesis Reconstruction. *Phys. Med. Biol* 2012; 57(12): 3915–3930.

[8] D. M. Pelt and K. J. Batenburg. Fast tomographic reconstruction from limited data using artificial neural networks. *IEEE Trans. Image Process.* 2013; 22(12): 5238–5251.

[9] D. M. Pelt and K. J. Batenburg. Improving Filtered Backprojection Reconstruction by Data-Dependent Filtering. *IEEE Trans. Image Process.* 2014; 23(11): 4750–4762.

[10] H. Kunze et al. Filter determination for Tomosynthesis aided by iterative reconstruction techniques. *Proc. of Fully3D* 2007: 309–312.

[11] P. M. Joseph. An improved algorithm for reprojecting rays through pixel images. *IEEE Trans. Med. Imag.* 1982; 1(3): 192–196.

[12] W. J. Palenstijn, K. J. Batenburg, and J. Sijbers. Performance improvements for iterative electron tomography reconstruction using graphics processing units (GPUs). *J. Struct. Biol.* 2011; 176(2): 250–253.